

Generalized Onsager-Regularized Lattice Boltzmann Method for error-free Navier-Stokes models on standard lattices

Anirudh Jonnalagadda,^{1,2,*} Walter Rocchia,¹ and Sauro Succi^{2,3,4}

¹*Computational mOdeling of NanosCaLE and bioPhysical sysTEms (CONCEPT) Lab, Istituto Italiano di Tecnologia, 16152 Genova, Italy*

²*Center for Life Nano- & Neuro-Science, Fondazione Istituto Italiano di Tecnologia, Viale Regina Elena 295, Rome, 00161, Italy*

³*Istituto per le Applicazioni del Calcolo, Consiglio Nazionale delle Ricerche, Via dei Taurini 19, Rome, 00185, Italy*

⁴*Department of Physics, Harvard University, 17 Oxford St., Cambridge, 02138, MA, USA*

(Dated: February 26, 2026)

This work presents a novel strategy to address Navier-Stokes modelling errors arising on first-nearest neighbour lattice Boltzmann (LB) methods and introduces fully local corrections through Onsager-Regularized (OReg) non-equilibrium populations. The proposed mechanism, which admits partially and completely corrected OReg models, is used to develop representative partially and completely corrected models for the six-moment-constrained guided equilibrium (GEq) representation on the D2Q9 lattice. The former realization only addresses compatibility condition violations and improves the accuracy by two/four orders of magnitude at reference/arbitrary lattice temperatures respectively, while the latter additionally corrects stress tensor modelling errors, resulting in a fully corrected exact model. Numerical benchmarks of the corrected schemes demonstrate improved accuracy and stability in comparison to the Lattice-BGK and uncorrected OReg-GEq schemes thus presenting a promising avenue for OReg based thermohydrodynamic extensions.

I. INTRODUCTION

The lattice Boltzmann (LB) method is a mesoscopic computational framework in which molecular collisions emulated at individual grid nodes are followed by the propagation of information to corresponding nearest-neighbours [1, 2]. For single relaxation time (SRT) schemes, these operations are mathematically expressed through the lattice Boltzmann equation (LBE):

$$f_i^*(x_\alpha, t) = f_i^{(eq)}(x_\alpha, t) + \left(1 - \frac{1}{\tau}\right) f_i^{(neq)}(x_\alpha, t), \quad (1a)$$

$$f_i^*(x_\alpha, t) = f_i(x_\alpha + c_{i_\alpha} \Delta t, t + \Delta t) \quad (1b)$$

where f_i^* represent the post-collision populations and the population set $\{f_i : i \in [0, Q]\}$ is defined on stencils comprising of Q lattice entries each having a D -dimensional lattice velocity c_{i_α} . The quantities $f_i^{(eq)}$ and $f_i^{(neq)} = (f_i - f_i^{(eq)})$ correspond to the equilibrium and non-equilibrium populations respectively, while the BGK relaxation time, $\tau = \nu/\theta$, is the ratio of the lattice viscosity, ν , to the reduced temperature θ . The corresponding macroscopic mass and momentum densities are obtained from the lattice populations as $\rho = \sum_i f_i$

and $\rho u_\alpha = \sum_i c_{i_\alpha} f_i$ respectively. The LB algorithm presented in Equation (1), which inherently involves localized non-linear collisions and linear non-local propagations, is particularly well suited to harness the power of modern compute infrastructures [3]. Indeed, successful

applications in numerous scientific and commercial settings have led to a significant uptake of LB schemes as an alternative computational fluid dynamics methodology.

Traditionally, LB schemes have operated with standard, first-nearest-neighbour discrete velocity spaces (Figure 1). However, since such lattices employ only three discrete speeds, $c_{i_\alpha} \in (0, \pm 1)$, certain higher-order moments degenerate into lower-order representations. As a result, standard-lattice LB models lose Galilean invariance, and can, therefore, only approximate the Navier-Stokes (NS) equations [4–6]. Consequently, such models are best suited for isothermal subsonic applications operating at the standard lattice reference temperature $\theta_0 = 1/3$. Indeed, for flows characterized by appreciable speeds and/or thermal fluctuations, the NS modelling errors arising on standard lattices produce grossly inaccurate results and often yield catastrophically unstable simulations.

Two strategies have been widely explored for enabling simulations of high speed flow phenomena within the LB framework. The first identifies the under-represented standard lattice velocity space as the source of the NS modelling errors, and takes the intuitive route of employing larger, multispeed, velocity sets [7–16]. However, multispeed lattices are accurate only over small ranges of temperature [17] and, due to the large number of discrete velocities required to completely recover compressible NS dynamics, incur significantly high computational costs. In the second, more direct, strategy, NS modelling errors are evaluated using the Chapman-Enskog (CE) multi-scale expansion procedure, and are eliminated by injecting correction populations into the LBE either via modified equilibrium representations [18, 19] or as explicit source terms [20–28]. However, it is important to note that the complexity of the correction populations are directly influenced by the analytical representation of

* Corresponding author: anirudh.jonnalagadda@iit.it

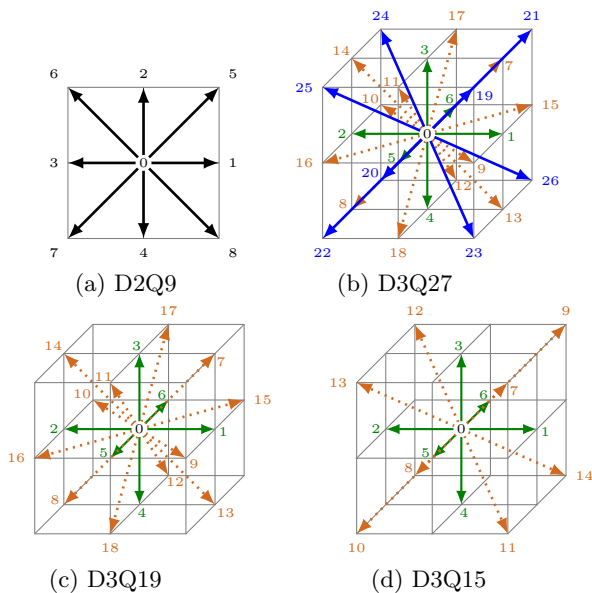


FIG. 1. 2D and 3D Standard lattices(color online).

the NS modelling errors. Specifically, using closure procedures based on the evolution equations for the stress tensor and heat flux vector in the CE expansion, these errors manifest in terms of the gradients of higher-order equilibrium moments. Usually, these error contributions can only be evaluated non-locally [29]. Thus the direct approach also compromises the computational efficiency of standard lattices.

It can be appreciated that an ideal compressible LB model would endeavour not only to retain the computational advantages of standard lattices, but also to allow for fully local representations of the correction terms. Here, the first effort towards this ideal is presented in the context of two-dimensional isothermal flow scenarios via the Onsager-Regularized (OReg) LB scheme [30–34]. We highlight that the proposed correction mechanism differs from existing approaches in the following ways. The first distinction lies in the significantly simpler mathematical representation of the OReg modelling errors. Specifically, since the momentum transport equation in the CE expansion is closed by directly evaluating the stress tensor in terms of the OReg non-equilibrium populations, the corresponding OReg modelling errors have the generic product form $\tilde{\mathbf{E}} = \mathbf{X}_{\alpha\beta} \cdot \phi(\Phi'_{\alpha\beta})$, where, $\mathbf{X}_{\alpha\beta} = \mathbf{S}_{\alpha\beta}/\theta$, with $\mathbf{S}_{\alpha\beta} = (\partial_\alpha u_\beta + \partial_\beta u_\alpha)/2$ being the strain rate tensor, is the non-equilibrium thermodynamic force associated with viscous processes, and ϕ is a scalar/vector function of the deviations of equilibrium moments from their Maxwell-Boltzmann (MB) counterparts $\Phi'_{\alpha\beta}$. Note that $\Phi'_{\alpha\beta}$ is an explicit function of the macroscopic field variables, and can be trivially evaluated once the equilibrium representation is fixed. Similarly, $\mathbf{X}_{\alpha\beta}$ can be locally evaluated through the definition of the incompressible stress tensor [30–32]. Thus, the second, and most important, distinction of the proposed OReg-based correction scheme is its amenability to yield fully-local correction populations. The third differentiating aspect

of the proposed correction mechanism lies in the type of modelling errors that are eliminated. It is important to note that the isothermal NS modelling errors on standard lattices emerge from two mutually independent sources, namely, erroneous stress-tensor representations as well as compatibility condition violations [34]. The proposed OReg-based correction procedure can address either of the two error sources and is, thus, able to yield partially or completely corrected isothermal OReg kinetic models. Note that such partially corrected models, which further improve the accuracy offered by the OReg scheme, are expected to be useful in scenarios involving small deviations from the lattice reference temperature; the fully corrected models serve as stepping stones towards OReg-based standard lattice compressible LB models.

The remainder of the manuscript is laid out as follows: Section II describes the uncorrected isothermal OReg scheme along with its hydrodynamic limit and NS modelling errors. The OReg-correction framework is then presented in an equilibrium- and stencil-agnostic setting in Section III. The proposed framework is then deployed for the D2Q9 guided-equilibrium (GEq) representation [20–22] in Section IV, and a representative partially corrected model, that improves the accuracy of the OReg-GEq scheme from $\mathcal{O}(u)$ and $\mathcal{O}(u^3)$ at $\theta \neq 1/3$ and $\theta = 1/3$ to $\mathcal{O}(u^5)$ at all for isothermal lattice temperatures, along with a completely corrected, exact OReg-GEq model for NS macrodynamics is presented. In Section V, the behaviour of the proposed corrected OReg-GEq models are evaluated against the uncorrected OReg-GEq scheme as well as the standard LBGK scheme for two canonical quasi 1D problems and in a non-linear 2D setting, namely the rotated decaying shear wave, isothermal shocktube, and doubly-periodic shear layer problems. Lastly, Section VIII presents our conclusions.

II. THE ONSAGER REGULARIZED SCHEME

The OReg scheme approaches LB through the lens of nonequilibrium thermodynamics and has empirically alluded to improved NS kinetic models on standard lattices [31, 33]. Indeed, recent theoretical investigations have explained these empirical findings by demonstrating an order-of-magnitude accuracy improvement in isothermal dynamics, despite abandoning the customary assumption of compliance with compatibility conditions at the NS level [34]. In the isothermal OReg formulation for monatomic gases [31, 34], the non-equilibrium populations used in Equation (1) are corrected from $f_i^{(neq)} = (f_i - f_i^{(eq)})$ to f_i^{OReg} and are given as:

$$f_i^{\text{OReg}} = \frac{f_i^{(eq)}}{2\rho\theta^2} \left(C_{i_\alpha} C_{i_\beta} - \frac{C_i^2}{D} \delta_{\alpha\beta} \right) + \sum_{k=0}^{Q-1} \left(c_{k_\alpha} c_{k_\beta} - \frac{c_k^2}{D} \delta_{\alpha\beta} \right) f_i^{(neq)}, \quad (2)$$

where $C_{i\alpha} = (c_{i\alpha} - u_\alpha)$ and $\delta_{\alpha\beta}$ is the Kronecker delta function. With equilibrium representations that satisfy fundamental constraints of

$$\sum_i f_i^{(eq)} = \rho \text{ and } \sum_i c_{i\alpha} f_i^{(eq)} = \rho u_\alpha, \quad (3)$$

and recover the MB equilibrium pressure tensor with an ideal gas equation of state,

$$\Pi_{\alpha\beta}^{(eq)} = \Pi_{\alpha\beta}^{\text{MB}} = \sum_i c_{i\alpha} c_{i\beta} f_i^{(eq)} = \rho(u_\alpha u_\beta + \theta \delta_{\alpha\beta}), \quad (4)$$

a generic, assumption free, CE expansion of the OReg lattice Boltzmann equation at the NS level yields the following equations in the macroscopic limit [34]:

$$\partial_t \rho + \partial_\alpha (\rho u_\alpha) = \partial_\alpha \left[\left(1 - \frac{\Delta t}{2\tau}\right) \psi_\alpha \right], \quad (5a)$$

$$\begin{aligned} \partial_\alpha (\rho u_\alpha) + \partial_\beta \Pi_{\alpha\beta}^{\text{MB}} + \partial_\beta \left[\left(1 - \frac{\Delta t}{2\tau}\right) \Pi_{\alpha\beta} \right] \\ = -\frac{1}{\tau} \psi_\alpha - \partial_t \left[\left(1 - \frac{\Delta t}{2\tau}\right) \psi_\alpha \right]. \end{aligned} \quad (5b)$$

The quantities ψ_α and $\Pi_{\alpha\beta}$ are the first order compatibility condition contributions and the OReg stress tensor representation respectively. Explicitly, ψ_α and $\Pi_{\alpha\beta}$ are given as [34]:

$$\psi_\gamma = \sum_i c_{i\gamma} f_i^{\text{OReg}} = -\tau \left(Q'_{\alpha\beta\gamma} - \frac{\delta_{\alpha\beta}}{D} q'_\gamma \right) X_{\alpha\beta}, \quad (6a)$$

$$\begin{aligned} \Pi_{\alpha\beta} = \sum_i c_{i\alpha} c_{i\beta} f_i^{\text{OReg}} = \underbrace{-\tau \rho \theta \left(\partial_\alpha u_\beta + \partial_\beta u_\alpha - \frac{2}{D} \partial_\chi u_\chi \delta_{\alpha\beta} \right)}_{\Pi_{\alpha\beta}^{\text{NS}}} \\ - \tau \underbrace{\left[R'_{\alpha\beta\gamma\mu} - u_\gamma Q'_{\alpha\beta\mu} - u_\mu Q'_{\alpha\beta\gamma} - \frac{\delta_{\gamma\mu}}{D} (R'_{\alpha\beta\chi\chi} - 2u_\chi Q'_{\alpha\beta\chi}) \right]}_{\tilde{\Pi}_{\alpha\beta}} X_{\gamma\mu}, \end{aligned} \quad (6b)$$

where, q'_α , $Q'_{\alpha\beta\gamma}$, and $R'_{\alpha\beta\gamma\mu}$ represent, respectively, the deviations of the heat flux vector, the third-order and the fourth-order moments from their MB counterparts.

It can be appreciated that Equations (5) represent approximate mass and momentum conservation equations in which modelling errors arise due to non-zero values of the deviations $\{\psi_\alpha, \tilde{\Pi}_{\alpha\beta}\}$. In the next section, we describe a how these deviations are eliminated in the generalized OReg framework.

III. ONSAGER-REGULARIZED CORRECTION FRAMEWORK

To obtain the desired corrected NS representations, we begin by introducing correction populations, Ψ_i , in the OReg populations and define a generalized non-equilibrium representation as $f_i^{\text{GOReg}} = f_i^{\text{OReg}} + \Psi_i$. Note that such a generalization is equivalent to introducing a correcting source term $S_C = (1 - \frac{1}{\tau}) \Psi_i$ into Equation (1). Nevertheless, we retain the interpretation of augmented OReg non-equilibrium populations in the ensuing discussions. To comply with the compatibility conditions and recover the NS stress tensor exactly, these newly defined f_i^{GOReg} populations must satisfy the following conditions:

$$\sum_i \{1, c_{i\alpha}, c_{i\alpha} c_{i\beta}\} f_i^{\text{GOReg}} = \{0, 0, \Pi_{\alpha\beta}^{\text{NS}}\}, \quad (7)$$

which directly impose the following constraints on Ψ_i :

$$\sum_i \{1, c_{i\alpha}, c_{i\alpha} c_{i\beta}\} \Psi_i + \{0, \psi_\alpha, \tilde{\Pi}_{\alpha\beta}\} = \{0, 0, 0\}. \quad (8)$$

It is noteworthy that Equation (8), which corresponds to 6 and 10 equations for the standard D2Q9 and D3Q15/19/27 lattices respectively, forms an under-determined system in both two- and three-dimensions. Thus, an infinite family of corrected OReg models can be obtained. Additionally, by relaxing the deviation set from $\{\psi_\alpha, \tilde{\Pi}_{\alpha\beta}\}$ to $\{\psi_\alpha, 0\}$, we can also obtain partially corrected approximate models having, in comparison to the uncorrected OReg scheme, further improved accuracies.

Note that the correction populations require numerical representations of ψ_α and $\tilde{\Pi}_{\alpha\beta}$ which, from Equation (6) can be seen that to have the product form $\tilde{\mathbb{E}}$ described in Section I. However, we highlight that the compatibility condition error can be evaluated directly since ψ_α is a moment of the known f_i^{OReg} populations. Thus, obtaining fully-local partially corrected OReg models is a straightforward exercise. For evaluating $\tilde{\Pi}_{\alpha\beta}$, this work leverages the interpretation of f_i^{OReg} being a one-step correction to $f_i^{(neq)}$ [34] and approximates $X_{\alpha\beta}$ locally via the first order accurate incompressible stress tensor:

$$\begin{aligned} \sigma = \tau \rho \theta (\partial_\alpha u_\beta + \partial_\beta u_\alpha) \\ \approx - \sum_i \left(c_{i\alpha} c_{i\beta} - \frac{c_i^2}{D} \delta_{\alpha\beta} \right) f_i^{\text{OReg}}. \end{aligned} \quad (9)$$

IV. CORRECTED 2D ONSAGER REGULARIZED MODELS

Here we present realizations of both fully corrected and partially corrected OReg schemes for the D2Q9 lattice using the guided equilibrium obtained from an entropic minimization procedure constrained to exactly recover

Equations (3) and (4) [20–22]. Explicitly, the guided equilibrium is given as:

$$f_i^{(eq)} = \rho \prod_{\alpha=x,y} \frac{(1 - 2c_{i\alpha}^2)}{2c_{i\alpha}^2} [c_{i\alpha}^2 - 1 + c_{i\alpha} u_\alpha + u_\alpha^2 + \theta]. \quad (10)$$

When used within the OReg framework, the corresponding expressions for ψ_α and $\tilde{\Pi}_{\alpha\beta}$ are obtained as:

$$\psi_\alpha^{\text{OReg|GEq}} = \frac{\tau \rho u_\alpha}{2\theta} (u_\alpha^2 + 3\theta - 1) \left(\partial_\alpha u_\alpha - \frac{1}{2} \partial_\chi u_\chi \right) \sim \begin{cases} \mathcal{O}(u^5) & \text{if } \theta = 1/3 \\ \mathcal{O}(u^3) & \text{otherwise} \end{cases} \quad (11a)$$

$$\tilde{\Pi}_{\alpha\beta}^{\text{OReg|GEq}} = \frac{\rho\tau}{2\theta} (\partial_x u_x - \partial_y u_y) \begin{cases} - [\theta(1-3\theta) + u_x^2(u_x^2-1)] & \text{if } \alpha = \beta = x \\ [\theta(1-3\theta) + u_y^2(u_y^2-1)] & \text{if } \alpha = \beta = y \\ u_x u_y (u_x^2 - u_y^2) & \text{if } \alpha \neq \beta. \end{cases} \quad (11b)$$

The prefactor in Equation (11b) is computed using Equation (9) as:

$$\frac{\rho\tau}{2\theta} (\partial_x u_x - \partial_y u_y) = -\frac{1}{4\theta^2} \sum_i (c_{i_x}^2 - c_{i_y}^2) f_i^{\text{OReg|GEq}}. \quad (12)$$

Earlier work demonstrated that $\tilde{\Pi}_{\alpha\beta}^{\text{OReg|GEq}}$ can be assimilated within $\Pi_{\alpha\beta}^{\text{NS}}$ to yield an $\mathcal{O}(u^3)/(u)$ accurate, variable viscosity representation of NS hydrodynamics when operating at the lattice reference temperature $\theta_0 = 1/3$ and arbitrary temperatures respectively [34]. In this representation, the OReg-GEq stress tensor takes the following $\mathcal{O}(u^5)$ accurate variable viscosity form:

$$\Pi_{\alpha\beta}^{\text{OReg|GEq}} = -(\tau\rho\theta) \mu_{\alpha\beta}^{\text{OReg}} (\partial_\alpha u_\beta + \partial_\beta u_\alpha - \partial_\chi u_\chi \delta_{\alpha\beta}) + \bar{\delta}_{\alpha\beta} \mathcal{O}(u^6) \quad (13a)$$

where,

$$\mu_{\alpha\beta}^{\text{OReg}} = \begin{cases} \frac{1}{2\theta^2} (\theta - u_\alpha^2)(1 - \theta - u_\alpha^2) & \text{if } \alpha = \beta \\ 1 & \text{otherwise,} \end{cases} \quad (13b)$$

and $\bar{\delta}_\alpha$ is the complement of the Kronecker delta that vanishes when $\alpha = \beta$. It is noteworthy that evaluating partially corrected populations Ψ_i^{P} that only eliminate $\psi_\alpha^{\text{OReg|GEq}}$ would yield a family of $\mathcal{O}(u^5)$ variable-viscosity kinetic models for the Navier-Stokes equations. One possible set of such correction populations are:

$$\Psi_i^{\text{P}} = -\frac{1}{2} \begin{cases} c_{i_\alpha} \psi_\alpha & \left\{ \begin{array}{l} \alpha = x \text{ if } i \in \{1, 3\}, \\ \alpha = y \text{ if } i \in \{2, 4\}, \end{array} \right. \\ 0 & \text{otherwise.} \end{cases} \quad (14)$$

Similarly, a realization of completely corrected populations Ψ_i^{C} that explicitly eliminate both $\psi_\alpha^{\text{OReg|GEq}}$ and $\tilde{\Pi}_{\alpha\beta}^{\text{OReg|GEq}}$ can be obtained as:

$$\Psi_i^{\text{C}} = -\frac{1}{4} \begin{cases} 0 & \text{if } i = 0, \\ -2 (\tilde{\Pi}_{\bar{\alpha}\bar{\alpha}} - c_{i_\alpha} \psi_\alpha) & \left\{ \begin{array}{l} \alpha = x \text{ if } i \in \{1, 3\}, \\ \alpha = y \text{ if } i \in \{2, 4\}, \end{array} \right. \\ (\tilde{\Pi}_{xx} + \tilde{\Pi}_{yy} + c_{i_\alpha} c_{i_{\bar{\alpha}}} \tilde{\Pi}_{xy}) & \text{otherwise.} \end{cases} \quad (15)$$

where $\bar{\alpha} = y$ if $\alpha = x$ and vice-versa. Note that the superscript OReg|GEq is dropped in both Equations (14) and (15) for better readability.

V. NUMERICAL RESULTS

A. Decaying shear wave

We first consider the numerical behaviour of the uncorrected, partially and completely corrected OReg models and present comparisons against that of the standard Lattice-BGK (LBGK) scheme for the quasi-1D benchmark simulation of a $\pi/4$ rotated decaying shear wave. Initialized on a 1×200 spatial grid with a unit density and a lattice viscosity of $\nu = 0.001$, the initial velocity field of the wave is given as:

$$u_x = u_y = \frac{\text{Ma}}{\sqrt{6}} + A_0 \sin \left[\frac{\sqrt{2}\pi}{N} (-x + y) \right], \quad (16)$$

where Ma is the Mach number, $A_0 = 0.001$ is the amplitude of the wave, and N is the spatial discretization in the y -direction. Note that while the same test case has been previously used for examining the uncorrected OReg-GEq formulation [34], the configurations examined in this work are significantly more severe. Specifically, in this study we consider both the x - and y -velocity components to be inclined, larger Mach number ranges, and multiple lattice temperatures. The numerical viscosity, $\tilde{\nu}$, are computed as described in [34] after 1200 iterations, and the deviation of $\tilde{\nu}$ from ν is reported in terms of the ratio $\tilde{\nu}/\nu$ in Figure 2 for four isothermal temperatures. Cases comprising catastrophic instabilities are represented with $\tilde{\nu}/\nu = 0$.

From Figure 2(a), it can be seen that while the LBGK scheme is consistently stable when the lattice temperature is maintained at $\theta = 0.25$, the associated numerical viscosity is incorrect at all considered Mach numbers.

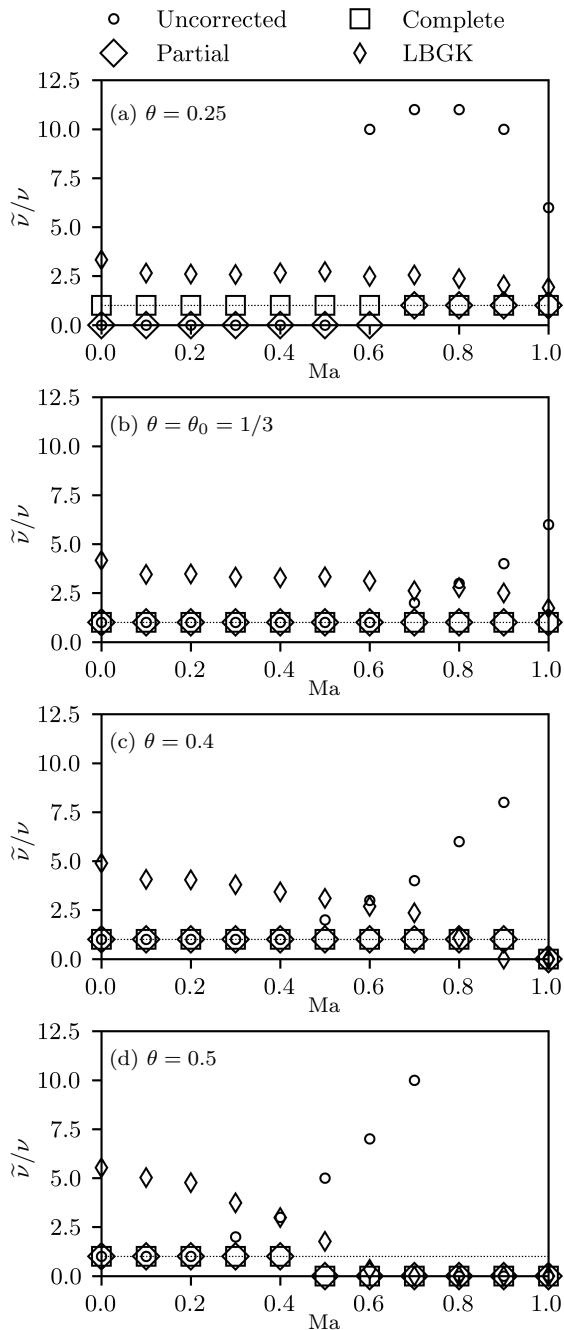


FIG. 2. Deviation of the numerical viscosity ($\bar{\nu}$) from the imposed viscosity ($\nu = 0.001$) in a decaying rotated shear wave. Results are presented for the Lattice BGK and the uncorrected, partially-corrected and, fully-corrected OReg schemes at different Mach numbers (Ma) and isothermal temperatures. Cases with catastrophic instabilities are represented with $\bar{\nu} = 0$ and the dotted line represents $\bar{\nu} = \nu$.

The uncorrected OReg scheme is not always stable, and, whenever stable, yields significantly larger values of numerical viscosity. The partially corrected OReg scheme slightly improves on the stability range of the uncorrected model and yields the correct numerical viscosity wherever stable. In contrast, the completely corrected OReg scheme yields accurate results in the entire range of con-

sidered Mach numbers.

In the remaining situations, as seen in Figures 2(b-d), the LBGK scheme shows a clear downward trend with the deviation in ν being large for small Ma and vice-versa. With the uncorrected OReg scheme, we see that the lattice viscosity is exactly recovered for a limited range of Mach numbers beyond which the deviation increases rapidly ultimately culminating into failure. Note that the maximum attainable Ma becomes smaller (0.6, 0.4 and 0.2) with increasing lattice temperature ($\theta = 1/3$, 0.4 and 0.5). In contrast, both the partially and completely corrected OReg schemes yield accurate viscosity values upto Ma = 1, 0.9 and 0.4 for the three considered lattice temperatures.

VI. ISOTHERMAL SHOCKTUBE

The uncorrected OReg-GEq formulation has also been evaluated previously using the quasi-1D isothermal shocktube benchmark case. Specifically, while it yielded accurate results without any spurious oscillations for two different configurations of lattice temperatures and viscosities, $(\theta, \nu) = (0.35, 10^{-5})$ and $(0.4, 10^{-9})$ respectively, the transition from the high-density to the equilibrated regions was found to be longer due to first-order accuracy at $\theta \neq 1/3$ [34]. Here, we employ an 800×1 grid with full-way bounce-back wall representations and consider two experiments to study the behaviour of the partially and completely corrected OReg schemes against that of the LBGK and uncorrected UC-OReg schemes. All simulations are run for 400 time steps.

In the first experiment, while the lattice temperature is maintained at $\theta = 0.4$ as in the previous study, the lattice viscosity is reduced by three decades to $\nu = 10^{-12}$. From Figure 3, it can be seen that the LBGK scheme yields significant numerical oscillations while the uncorrected OReg scheme is stable and free from spurious oscillations even at $\nu = 10^{-12}$ due to its variable viscosity nature. However, the uncorrected OReg scheme still retains the incorrect slope in the transition region as shown in Figures 3(i-iv). Further, in comparison to the analytical solution, the uncorrected OReg scheme recovers a slightly smaller equilibrated density (Figure 3(v)) while the equilibrated velocity (Figure 3(vi)) is exactly recovered. Finally, in the low-density region, Figures 3(vii, viii) reveal that the equilibrium region is slightly longer than expected. In contrast, both the partially and fully corrected OReg schemes accurately recover the density and velocity fields in the entire flow domain.

Figure 4 presents the results of the second experiment which, as in the previous study, maintains the lattice viscosity at $\nu = 10^{-9}$ but employs a higher lattice temperature of $\theta = 0.55$. It can be seen that the uncorrected OReg scheme, while stable, still retains all the deficiencies observed in the first experiment. In contrast, and like the previous case, both the partially and completely corrected OReg schemes address all deficiencies.

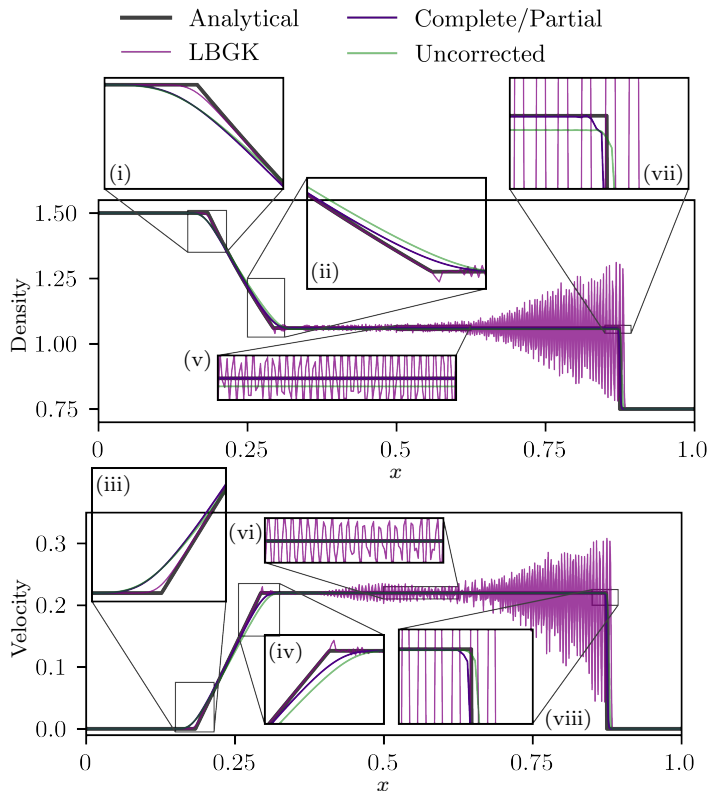


FIG. 3. Isothermal shocktube results for different LB schemes at a mildly elevated isothermal lattice temperatures ($\theta = 0.4$) and an extremely small lattice viscosity of $\nu = 1 \times 10^{-12}$.

We highlight that while the OReg schemes display numerical oscillations as shown in Figure 4(v, vi), the magnitude of these artefacts are negligible even at temperatures as high as $\theta = 0.55$. Conversely, the LBGK scheme yields unphysical results and, therefore, does not feature in Figure 4.

VII. DOUBLY PERIODIC SHEAR LAYER

The behaviours of both the proposed corrected OReg schemes have been indistinguishable from one another due to the quasi-1D nature of the two problems considered in the previous sections. Thus, in this section, we consider a purely two dimensional non-linear problem namely the doubly-periodic shear layer benchmark case. The $2\pi \times 2\pi$ simulation domain, discretized using N grid points in each direction, is initialized with unit density and a velocity field given as:

$$u_x = \begin{cases} u_0 \tanh \left[\kappa \left(\frac{y}{N} - \frac{1}{4} \right) \right], & y \leq \frac{N}{2} \\ u_0 \tanh \left[\kappa \left(\frac{3}{4} - \frac{y}{N} \right) \right], & y > \frac{N}{2} \end{cases} \quad (17a)$$

$$u_y = \delta u_0 \sin \left[2\pi \left(\frac{x}{N} + \frac{1}{4} \right) \right]. \quad (17b)$$

The parameters $\kappa = 80$ and $\delta = 0.05$ represent the width of the shear layers and the perturbation in the y -velocity

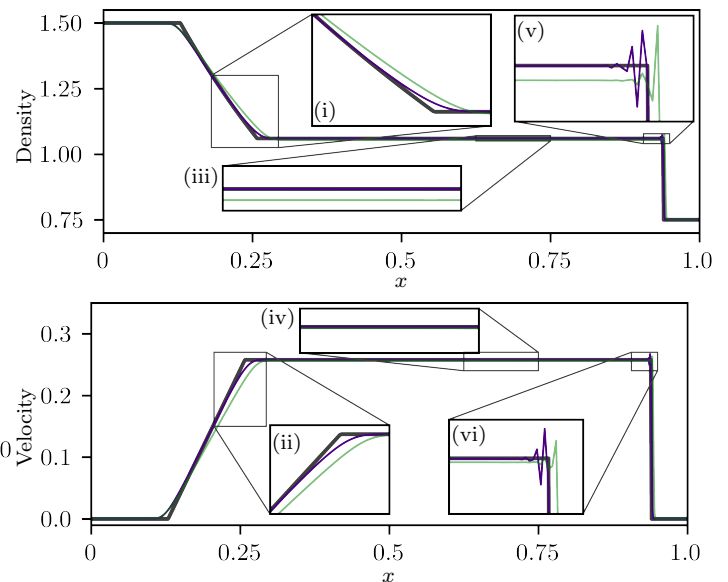


FIG. 4. Isothermal shocktube results for different LB schemes at an elevated isothermal lattice temperatures ($\theta = 0.55$) and lattice viscosity of $\nu = 1 \times 10^{-9}$. The represented curves have the same meaning as that of Figure 3. Note that the LBGK yield unphysical results for this case and is therefore not represented.

that initiates a Kelvin-Helmholtz instability. The system has a characteristic velocity $u_0 = 0.04$, and a Reynolds number $\text{Re} = (u_0 N)/\nu = 30000$. Simulations are run on three square grids of increasing size having side lengths $N = 128, 256$ and 512 grid points. Figures 5 and 6 represent vorticity contours at unit characteristic turnover time $t_c = N_{\text{iter}}/(N/u_0)$ for two isothermal temperatures $\theta = 0.4$ and 0.6 .

At $\theta = 0.4$, the uppermost panel of Figure 5 reveals that the LBGK scheme yields results that are unstable and contain three distinct spurious vortices in each arm on the smallest and intermediate grids respectively. Upon further refining the grid, the observed numerical artefacts are seen to vanish. We remark that the LBGK scheme behaves similarly even at the lattice reference temperature $\theta_0 = 1/3$, with the only difference being the formation of a single spurious vortex in the arms of the shear layer on the intermediate grid. This result is well known for the considered parameters and is therefore not presented here. In contrast, it can be seen that all three OReg schemes yield stable results even on the coarsest grid. From Figures 5(j-l), we see that the $\mathcal{O}(u/u^5)$ variable-viscosity uncorrected/partially corrected formulations and the completely corrected OReg scheme yield shear layers of progressively reducing thicknesses on the finest grid. These results clearly delineate the behaviour of the two proposed corrected OReg schemes and highlight the need for eliminating spurious contributions from the pressure tensor at elevated isothermal temperatures. However, it can be seen that the shear layers obtained with the completely corrected OReg scheme are still thicker than those from the LBGK

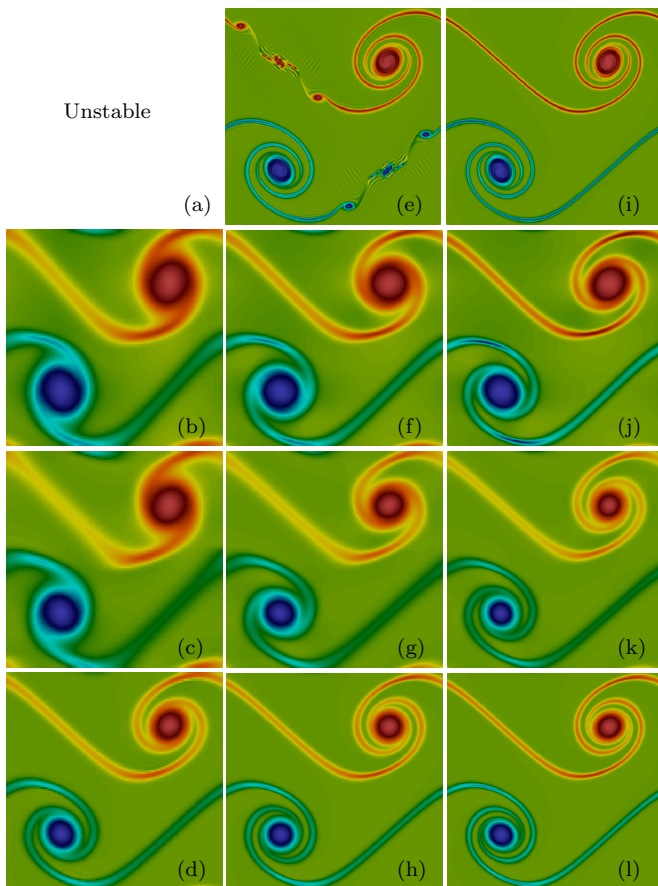


FIG. 5. Vorticity contours for the double periodic shear layer problem after unit characteristic time at an isothermal lattice temperature of $\theta = 0.4$. Simulations are conducted for the LBGK, uncorrected, partially-corrected and completely-corrected OReg schemes (top to bottom) on N^2 sized grids with $N = 128, 256$ and 512 (left to right).

scheme. This behaviour manifests due to numerical errors arising from evaluating derivatives through Equation (12). Indeed, while the first order approximation of the nonequilibrium viscous thermodynamic force $X_{\alpha\beta}$ using Equation (9) is the most likely culprit, further work is needed for improving local representations of $X_{\alpha\beta}$.

Nevertheless, the utility of the proposed corrected OReg schemes can be appreciated in the $\theta = 0.6$ case where the LBGK scheme is found to be unstable even on grids as large as $N = 2024$. Note that such a grid resolution nearly corresponds to DNS resolution for the considered Reynolds number of $Re = 30000$. As shown in Figure 6, the OReg schemes are stable on all the three for grids considered with the behaviour of the uncorrected, partially and fully corrected OReg schemes being similar to those observed in the $\theta = 0.4$ case.

VIII. CONCLUSION

In this work, we demonstrate the utility of the OReg LB scheme in addressing the Navier-Stokes modelling errors

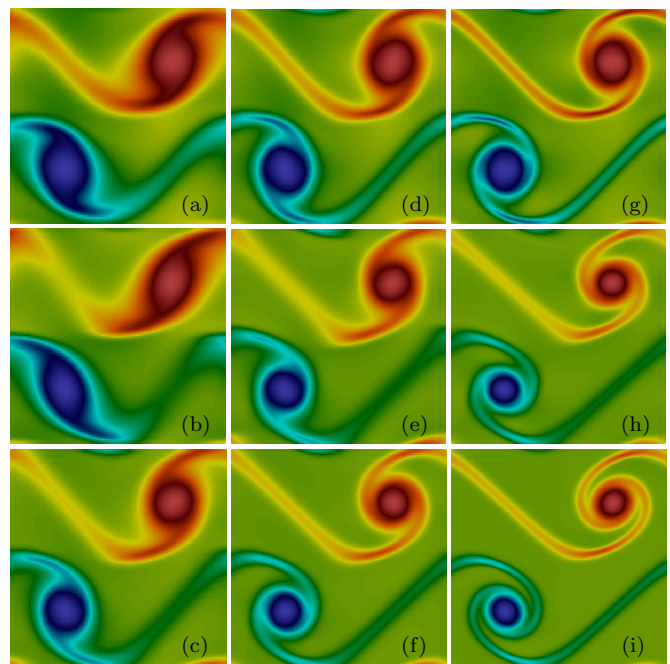


FIG. 6. Vorticity contours for the double periodic shear layer problem after unit characteristic time at an isothermal lattice temperature of $\theta = 0.6$. Simulations are conducted for the uncorrected, partially-corrected and completely-corrected OReg schemes (top to bottom) on N^2 sized grids with $N = 128, 256$ and 512 (left to right).

arising on standard lattices in a fully local manner and present a framework that eliminates errors arising from violations of constraints on non-equilibrium populations. The proposed framework deviates from existing strategies of extending the equilibrium distribution representation or introducing explicit source terms and modifies the non-equilibrium OReg populations with correction populations. Additionally, by reducing the the number of non-equilibrium constraint violations being corrected, we demonstrate that partially corrected OReg schemes with significantly improved NS modelling accuracy can be also obtained. We present realizations of partially and completely corrected OReg schemes and compare the proposed models against the Lattice BGK and uncorrected OReg schemes in quasi one-dimensional and non-linear two-dimensional settings. In comparison to the Lattice BGK scheme, all the considered OReg schemes yield better stability characteristics. Among the OReg schemes, the completely corrected OReg scheme is, as expected, found to yield the best accuracy followed by the partially corrected and the uncorrected OReg schemes. We highlight that, while the present study is conducted in the specific context of the D2Q9 guided equilibrium representation, the ideas presented in this work can be easily generalized to 3D standard stencils and other equilibrium representations for advanced use cases such as, e.g., phase-field [35] or fluctuating [36] LB models.

ACKNOWLEDGMENTS

Funded by the European Union - NextGenerationEU: This work has received funding from the European High Performance Joint Undertaking (J.U.) (Grant Agreement No. 101093169) and the Ministero delle Impresse e del Made in Italy (Grant No. P/040003/01-02/X64).

-
- [1] S. Succi, *The lattice Boltzmann equation: for complex states of flowing matter* (Oxford university press, 2018).
- [2] T. Krüger, Halim Kusumaatmaja, Alexandr Kuzmin, Or-est Shardt, Goncalo Silva, and Erlend Mahnus Viggen, *The Lattice Boltzmann Method: Principles and Practice*, 1st ed. (Springer International Publishing, 2017).
- [3] S. Succi, G. Amati, M. Bernaschi, G. Falcucci, M. Lauricella, and A. Montessori, Towards Exascale Lattice Boltzmann computing, *Computers & Fluids* **181**, 107 (2019).
- [4] Y. H. Qian, D. D’Humières, and P. Lallemand, Lattice BGK Models for Navier-Stokes Equation, *EPL (Europhysics Letters)* **17**, 10.1209/0295-5075/17/6/001 (1992).
- [5] Y. H. Qian and S. A. Orszag, Lattice bgk models for the navier-stokes equation: Nonlinear deviation in compressible regimes, *Europhysics Letters* **21**, 255 (1993).
- [6] I. Karlin and P. Asinari, Factorization symmetry in the lattice boltzmann method, *Physica A: Statistical Mechanics and its Applications* **389**, 1530 (2010).
- [7] F. J. Alexander, S. Chen, and J. D. Sterling, Lattice boltzmann thermohydrodynamics, *Phys. Rev. E* **47**, R2249 (1993).
- [8] T. Kataoka and M. Tsutahara, Lattice boltzmann model for the compressible navier-stokes equations with flexible specific-heat ratio, *Phys. Rev. E* **69**, 035701 (2004).
- [9] Q. Li, Y. L. He, Y. Wang, and W. Q. Tao, Coupled double-distribution-function lattice boltzmann method for the compressible navier-stokes equations, *Phys. Rev. E* **76**, 056705 (2007).
- [10] M. Watari, Finite difference lattice boltzmann method with arbitrary specific heat ratio applicable to supersonic flow simulations, *Physica A: Statistical Mechanics and its Applications* **382**, 502 (2007).
- [11] S. S. Chikatamarla and I. V. Karlin, Lattices for the lattice boltzmann method, *Phys. Rev. E* **79**, 046701 (2009).
- [12] S. S. Chikatamarla and I. V. Karlin, Entropy and galilean invariance of lattice boltzmann theories, *Phys. Rev. Lett.* **97**, 190601 (2006).
- [13] X. Shan, The mathematical structure of the lattices of the lattice boltzmann method, *Journal of Computational Science* **17**, 475 (2016), discrete Simulation of Fluid Dynamics 2015.
- [14] M. Atif, M. Namburi, and S. Ansumali, Higher-order lattice Boltzmann model for thermohydrodynamics, *Phys. Rev. E* **98** (2018).
- [15] P. K. Kolluru, M. Atif, M. Namburi, and S. Ansumali, Lattice Boltzmann model for weakly compressible flows, *Phys. Rev. E* **101** (2020).
- [16] M. Atif, N. H. Maruthi, P. K. Kolluru, C. Thantapanally, and S. Ansumali, Lattice boltzmann model for transonic flows, *Physics of Fluids* **37**, 116134 (2025).
- [17] N. Frapolli, *Entropic lattice Boltzmann models for thermal and compressible flows*, Ph.D. thesis, ETH Zurich (2017).
- [18] M. H. Saadat, B. Dorschner, and I. Karlin, Extended lattice boltzmann model, *Entropy* **23**, 10.3390/e23040475 (2021).
- [19] M. H. Saadat, S. A. Hosseini, B. Dorschner, and I. V. Karlin, Extended lattice boltzmann model for gas dynamics, *Physics of Fluids* **33**, 046104 (2021).
- [20] N. I. Prasianakis and I. V. Karlin, Lattice boltzmann method for thermal flow simulation on standard lattices, *Phys. Rev. E* **76**, 016702 (2007).
- [21] N. I. Prasianakis and I. V. Karlin, Lattice boltzmann method for simulation of compressible flows on standard lattices, *Phys. Rev. E* **78**, 016704 (2008).
- [22] N. I. Prasianakis, I. V. Karlin, J. Mantzaras, and K. B. Boulouchos, Lattice boltzmann method with restored galilean invariance, *Phys. Rev. E* **79**, 066702 (2009).
- [23] Q. Li, K. H. Luo, Y. L. He, Y. J. Gao, and W. Q. Tao, Coupling lattice boltzmann model for simulation of thermal flows on standard lattices, *Phys. Rev. E* **85**, 016710 (2012).
- [24] Y. Feng, P. Sagaut, and W. Tao, A three dimensional lattice model for thermal compressible flow on standard lattices, *Journal of Computational Physics* **303**, 514 (2015).
- [25] M. H. Saadat, F. Bösch, and I. V. Karlin, Lattice boltzmann model for compressible flows on standard lattices: Variable prandtl number and adiabatic exponent, *Phys. Rev. E* **99**, 013306 (2019).
- [26] S. Guo, Y. Feng, J. Jacob, F. Renard, and P. Sagaut, An efficient lattice boltzmann method for compressible aerodynamics on d3q19 lattice, *Journal of Computational Physics* **418**, 109570 (2020).
- [27] Y. Feng, P. Boivin, J. Jacob, and P. Sagaut, Hybrid recursive regularized thermal lattice boltzmann model for high subsonic compressible flows, *Journal of Computational Physics* **394**, 82 (2019).
- [28] S. A. Hosseini, N. Darabiha, and D. Thévenin, Compressibility in lattice boltzmann on standard stencils: effects of deviation from reference temperature, *Philosophical Transactions of the Royal Society A* **378**, 20190399 (2020).
- [29] M. Lauricella, A. Tiribocchi, S. Succi, L. Brandt, A. Mukherjee, M. La Rocca, and A. Montessori, Thread-safe multiphase lattice boltzmann model for droplet and bubble dynamics at high density and viscosity contrasts, *Physics of Fluids* **37**, 072111 (2025).
- [30] A. Jonnalagadda, A. Sharma, and A. Agrawal, Revisiting the Lattice Boltzmann Method Through a Nonequilibrium Thermodynamics Perspective, *Journal of Heat Transfer* **143** (2021), 052102.
- [31] A. Jonnalagadda, A. Sharma, and A. Agrawal, Onsager-regularized lattice boltzmann method: A nonequilibrium thermodynamics-based regularized lattice boltz-

- mann method, Phys. Rev. E **104**, 015313 (2021).
- [32] A. Jonnalagadda, A. Sharma, and A. Agrawal, On application of the regularized lattice boltzmann method for isothermal flows with non-vanishing knudsen numbers, Numerical Heat Transfer, Part B: Fundamentals **84**, 756 (2023).
- [33] D. Galbiati, *On Onsager-consistent regularization in the lattice Boltzmann method for accurate simulation of turbulent vortex flows*, Master's thesis, Politecnico di Milano, Milano, Italy (2024).
- [34] A. Jonnalagadda, A. Agrawal, A. Sharma, W. Rocchia, and S. Succi, Towards nonlinear thermohydrodynamic simulations via the onsager-regularized lattice-boltzmann method, Phys. Rev. Res. **7**, 033286 (2025).
- [35] I. Rasin, W. Miller, and S. Succi, Phase-field lattice kinetic scheme for the numerical simulation of dendritic growth, Phys. Rev. E **72**, 066705 (2005).
- [36] M. Lauricella, A. Montessori, A. Tiribocchi, and S. Succi, Regularized fluctuating lattice boltzmann model, The Journal of Chemical Physics **163**, 164102 (2025).